Investigating the electronic origins of the repulsion between substitutional and interstitial solutes in hcp Ti

N. S. Harsha Gunda ⬤, Carlos G. Levi ⬤, and Anton Van der Ven[*]

Materials Department, University of California, Santa Barbara, California 93117, USA

The high solubility of oxygen in Ti, Zr, and Hf makes it difficult to stabilize protective oxide scales on their surfaces as the subsurface regions can serve as boundless sinks that continuously dissolve oxygen. Alloying elements are crucial to reduce the oxygen solubility and diffusivity within early transition metals. Past studies have shown that most substitutional alloying additions to titanium repel interstitial oxygen. Here we use first-principles calculations to show that this repulsion is short ranged and explore several factors that are likely responsible for the repulsive interaction. Calculations of Bader charges suggest the existence of short-range Coulomb interactions due to the accumulation of charge on the substitutional solute and interstitial oxygen that is drawn from the Ti host. Misfit strains due to differences in the atomic radii of the solutes and Ti are also found to play a role. We identify a unique hybridization phenomenon between dissolved substitutional elements and interstitial oxygen within hcp Ti that leads to a repulsive interaction at short distances, similar to that between closed-shell atoms, which is especially pronounced for Al and Si solutes.

I. INTRODUCTION

Early transition metals belonging to groups 4 and 5 of the periodic table (Ti, Zr, Hf, V, Nb, and Ta) are able to dissolve high concentrations of interstitial species such as oxygen, nitrogen, and carbon and form a rich family of oxides, nitrides, and carbides [1–13]. Ti, Zr, and Hf in particular can dissolve oxygen over the interstitial sites of their hcp crystal structure up to an atom fraction of 0.33. This high solubility not only affects mechanical properties [14–16] but makes it almost impossible to sustain a protective oxide scale on their surfaces as the scale is continuously undermined from below [17–21]. Alloying strategies are therefore essential to enable the stabilization of an oxide scale on metals such as titanium. The alloying additions play several roles. They may alter the types of oxide phases that form during oxidation [22–25]. They can also reduce the oxygen solubility and oxygen mobility in the base metal [21,26,27].

A first-principles study by Wu and Trinkle [26] predicted that almost every element of the periodic table when substitutionally dissolved in hcp Ti will repel interstitial oxygen. The repulsion increases when going to the right in the periodic table. Alloying elements such as Al and Si are predicted to have especially large and repulsive binding energies with interstitial oxygen that are on the order of 0.8 to 1 eV, respectively. This repulsion is surprising considering that elemental Al and Si readily react with oxygen to form Al_2O_3 and SiO_2. A recent first-principles study of the Ti-Al-O ternary [27] confirmed the existence of a large repulsion between dissolved Al and oxygen in Ti and showed how this repulsion affects thermodynamic properties at elevated temperature.

Here we systematically investigate the origin of the repulsive interactions between interstitial oxygen and dissolved alloying elements within Ti using first-principles electronic structure calculations. We focus on a subset of the alloying elements considered by Wu and Trinkle and analyze the role of electronic structure, atomic relaxations, and charge redistribution between the host and solutes. Several distinct interactions are identified that have their origin in the unique electronic structure of a Ti host containing dilute interstitial oxygen. One interaction is electrostatic in nature and is short ranged, arising from a redistribution in charge between the Ti host and solutes. Another interaction can be attributed to a strain energy penalty due to a size mismatch between the solute and Ti. We also identify an interaction that arises from the hybridization between atomiclike orbitals on dissolved oxygen and substitutional solutes, resulting in a closed-shell type of repulsion at short distances. The insights generated by this study should also apply to oxygen-solute interactions in other early transition metals.

II. METHODS

First-principles electronic structure calculations were performed using density functional theory as implemented in the VASP plane-wave software package [28–31]. The exchange correlation functional was that of Perdew, Burke, and Ernzerhof (PBE) [32]. The projector augmented wave method (PAW) was used to describe interactions between valence and core electrons [33,34]. The valence states of the Al and Si PAW-PBE potentials were the $3s$ and $3p$ states, while those of O were the $2s$ and $2p$ states. For Ti and Fe, belonging to the $3d$ transition element series, the "sv" potentials with valence states $3s$, $3p$, $3d$, and $4s$ states were used. For Cr, the "pv" potential with $3p$, $3d$, and $4s$ valence states was used.
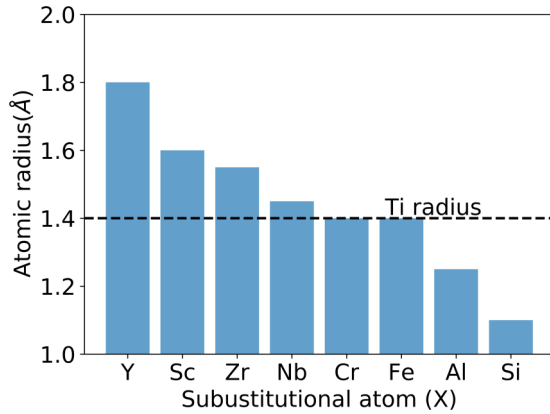
---

*avdv@ucsb.edu

FIG. 1. Atomic radii of alloying elements investigated in this study [39].

FIG. 2. The variation of the energy of hcp Ti as a substitutional solute X is moved away from the nearest-neighbor position of an interstitial oxygen. The reference state of the energy scale was set to the energy of the crystal when X and O are nearest neighbors at approximately 2 Å. A $3 \times 3 \times 3$ supercell of hcp was used to calculate these energies.

The sv potentials with $4s$, $4p$, $4d$, and $5s$ valence state were used for Y, Zr, and Nb in the $4d$ transition element series. All calculations were performed with a plane wave cutoff of 550 eV.

Calculations were performed using a $3 \times 3 \times 3$ supercell of hcp Ti with a Γ-centered $6 \times 6 \times 3$ k-point grid. The volume was held fixed at the equilibrium volume of pure Ti, while all atoms were allowed to fully relax until an energy convergence of 10^{-4} eV and a force convergence of 0.02 eV/Å on each atom was reached. We found that volume relaxations lead to a negligible change in the O-X binding energies (of the order of 10 meV). The Methfessel-Paxton (order 2) method was used to treat partial occupancies during relaxation runs, while the tetrahedron method with Blöchl corrections was used during static runs. Calculations with Cr and Fe were performed spin polarized. Bader charges were calculated with the scheme of Henkelman and colleagues [35–37]. The charge densities were visualized using the VESTA software [38].

III. RESULTS

We considered eight alloying elements from different parts of the periodic table with a range of atomic radii (Fig. 1) and valence electronic structure to investigate trends in the interactions between dilute substitutional solutes and octahedral oxygen in hcp Ti. Yttrium was chosen due to its strong affinity for oxygen and its tendency to form among the most stable oxides. Zirconium, niobium, and chromium were chosen as they are refractory transition metals and are commonly combined with Ti to form high-entropy alloys [40–44]. Crystalline Y, Zr, and Nb are also able to dissolve large concentrations of interstitial oxygen [1,6,9,45]. Iron is a representative of a later transition metal, while Al and Si are important alloying additions that are commonly added to metals to promote the formation of protective Al_2O_3 and SiO_2 scales [46–48]. We also included Sc as it is one of the few substitutional solutes that is predicted to exhibit a weak attraction to interstitial oxygen [26]. As is evident in Fig. 1, the atomic radii of the selected elements span a range of values relative to that of Ti, decreasing upon moving to the right in the periodic table.
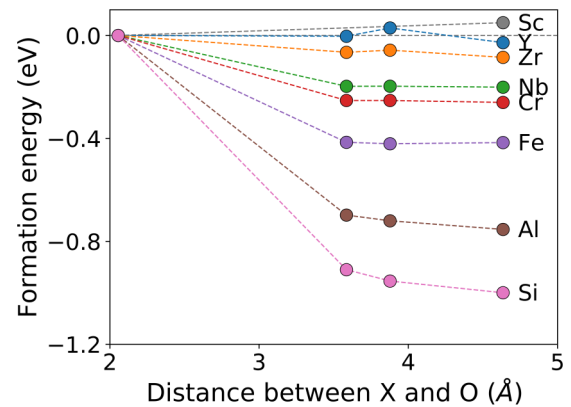
A. Substitutional solute-oxygen interaction is short ranged

The interaction between a substitutional solute X (Y, Sc, Zr, Nb, Cr, Fe, Al, and Si) and an interstitial O in hcp Ti was determined by calculating the energy of a $3 \times 3 \times 3$ supercell of the hcp unit cell as a function of the X-O separation. The interstitial oxygen is coordinated by six substitutional sites. Figure 2 shows the variation of the energy of the cell with increasing X-O distance. The energy for the nearest-neighbor configuration in which the solute occupies a site that directly coordinates the interstitial oxygen atom at a distance of approximately 2 Å is used as the reference state and is set equal to zero. With the exception of Sc, Fig. 2 shows that the energy of the supercell decreases as the solute X is moved beyond the first-nearest-neighbor shell of the interstitial oxygen. This indicates that the interaction between the solute X and oxygen is repulsive. For most solutes, the energy varies negligibly beyond the second-nearest-neighbor distance at approximately 3.5 Å, indicating that the repulsion is very local and, for the most part, felt only within the first-nearest-neighbor shell.

The energies in Fig. 2 were calculated allowing for atomic relaxations. They therefore combine contributions from electronic interactions and the effects of local distortions due, for example, to a size mismatch between the solute and the Ti host. It is also instructive to inspect binding energies in the absence of atomic relaxations. Figure 3 shows calculated binding energies ΔE for each solute, defined as the difference in energy between the nearest-neighbor X-O configuration minus that of the fourth-nearest-neighbor configuration. Both relaxed (blue) and unrelaxed (orange) binding energies are shown. A positive binding energy signifies a repulsive interaction. Large differences between the relaxed and unrelaxed values are an indication of the importance of atomic relaxations in determining the binding energy ΔE.

Figure 3 shows that the effects of relaxations are the most pronounced for Y, Zr, and Si. The atomic radii of both Y and Zr are larger than the atomic radius of Ti, while that of Si is substantially smaller, as shown in Fig. 1. In the case of Y, relaxations appear to completely undo an otherwise
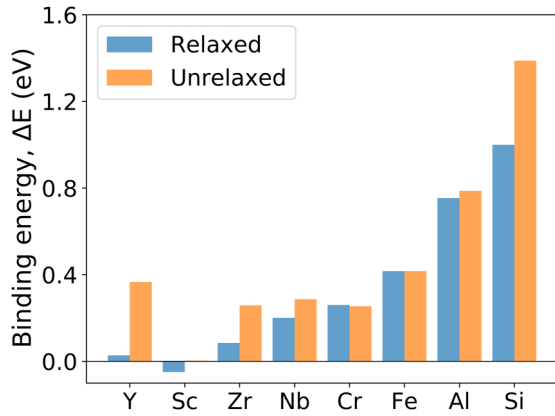
FIG. 3. Binding energies ΔE between different substitutional solutes (X = Y, Sc, Zr, Nb, Cr, Fe, Al, and Si) and interstitial O in hcp Ti. The energies were calculated as the difference in the energy of a Ti supercell when X and O are nearest neighbors and the energy when X and O are fourth-nearest neighbors. Positive values indicate a repulsive interaction between X and O. The relaxed ΔE values (blue) were calculated while allowing for atomic relaxations at constant volume.

repulsive interaction that exists when Y and O are at their ideal positions within hcp Ti. While Sc is larger than Ti, the unrelaxed binding energy is negligible (3 meV), and the effect of relaxation is also minimal but leads to a slightly negative (attractive) binding energy with oxygen. Figure 3 also shows that the binding energy between oxygen and alloying elements such as Cr, Fe, and Al is negligibly affected by relaxations. Both Cr and Fe have atomic radii that are very similar to that of Ti, while Al is slightly smaller.

One measure of the degree of relaxation is the equilibrium X-O bond distance when X and O are nearest neighbors. Figure 4 shows the relaxed X-O bond distances and compares them to the lengths of the Ti-O bond on the opposite side of O. With the exception of Cr, all other alloying elements have an X-O bond length that is larger than the opposing Ti-O bond length. The large X-O bond lengths indicate that O is pushed away from the solute X towards the Ti on the opposite side of the octahedral interstitial site containing O, resulting in a
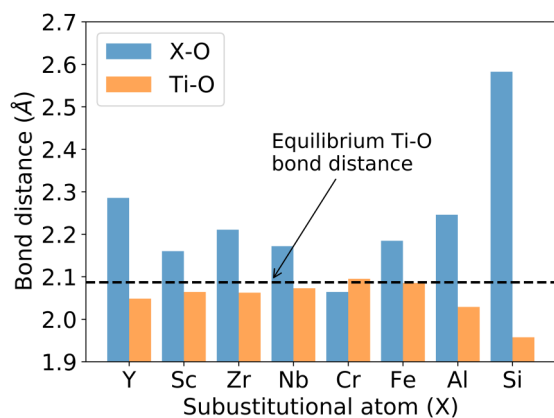

FIG. 4. Relaxed bond lengths between X and O and between Ti and O when X is in the nearest-neighbor shell of interstitial O.
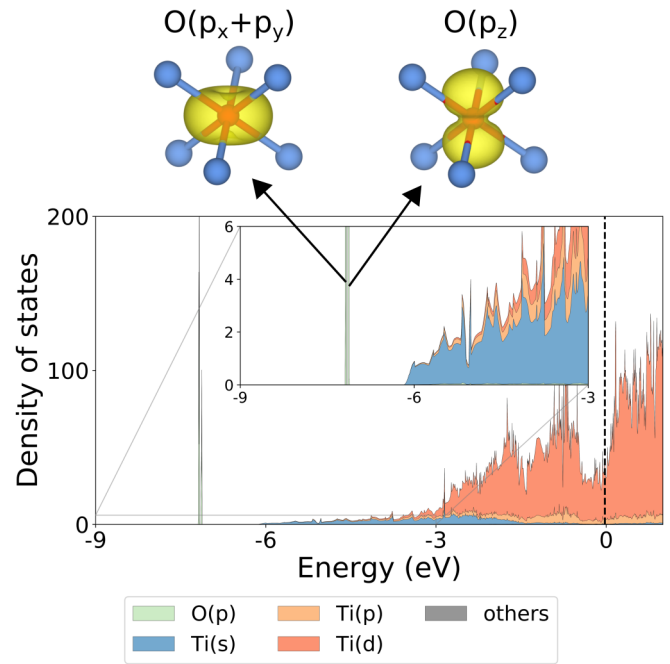

FIG. 5. The electronic densities of states (DOS) of a supercell of hcp Ti containing a single interstitial oxygen. The insets show the charge densities corresponding to the narrow spikes in the DOS at low energy.

shorted Ti-O bond. The relaxations are especially pronounced for Y, Zr, Al, and Si. While Y and Zr are larger than Ti, Al and Si are smaller. The large Al-O and Si-O bond lengths are therefore surprising and must arise from factors other than the intrinsic size of Al and Si. In the next section we will show that a rehybridization of atomiclike orbitals occurs when O becomes a nearest neighbor of either a Si or Al solute.

B. An analysis of the electronic structure

We next analyze changes in electronic structure as an alloying element X is brought into the nearest-neighbor shell of an oxygen atom residing in an octahedrally coordinated interstitial site of hcp Ti. It is instructive to first consider the electronic density of states (DOS) of a supercell of hcp Ti containing one interstitial oxygen in the absence of any other solutes. It is shown in Fig. 5, where the position of the Fermi level is denoted by the vertical dashed line. The electronic states having Ti s and d character are shown in blue and orange, respectively. The valence p levels of oxygen have energies that are far removed from the valence states of Ti derived from the $4s$ and $3d$ levels. Hence, there is very little hybridization between the oxygen p levels and the valence electrons of Ti, resulting in highly localized states around oxygen within a very narrow energy range, as shown in the calculated density of states plot in Fig. 5. Two very closely spaced peaks derived primarily from oxygen p states are evident. One resembles a p_z-like state, which is aligned along the c axis of the hcp crystal. The other resembles a superposition of the p_x and p_y orbitals that form a doughnut-shaped charge density parallel to the basal plane of the hcp crystal. Their charge densities are shown as insets in Fig. 5.
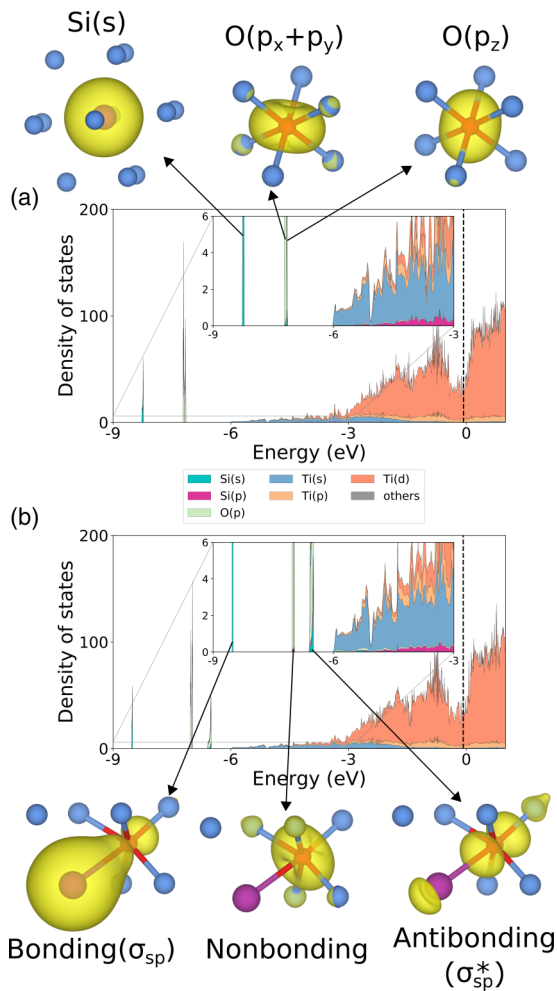
FIG. 6. (a) The DOS of a Ti supercell containing a single substitutional Si in the fourth nearest neighbor shell of an interstitial O. (b) The DOS of the same crystal when Si is in the nearest-neighbor shell of an interstitial O.
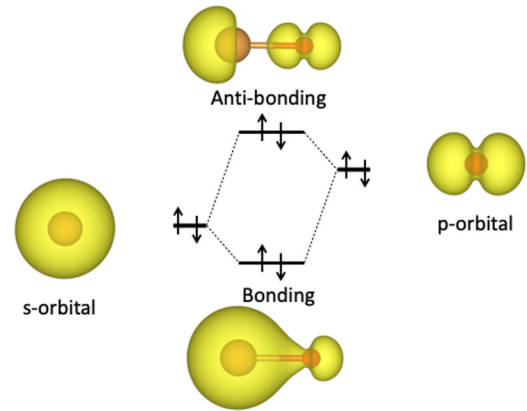

FIG. 7. Schematic hybridization diagram and charge densities that emerge when an s orbital and a p orbital combine to form bonding and antibonding orbitals.

Figure 6(a) shows the DOS for a supercell of Ti containing an interstitial oxygen and a substitutional Si placed in the fourth-nearest-neighbor shell of the oxygen. While the Si p states hybridize with the Ti valence states, the Si $2s$ states do not and remain highly localized, as illustrated in Fig. 6(a). Also evident in Fig. 6(a) are the oxygen p states, which are very similar to those of oxygen in pure Ti without a Si impurity. The energy of the Si s state is lower than that of the oxygen p states.

When Si is moved to the nearest-neighbor shell of oxygen, the local s-like state of Si interacts strongly with the p-like orbitals of oxygen. This is evident in the calculated DOS of Fig. 6(b) for a supercell of Ti in which a Si solute is a nearest neighbor of oxygen. Three separated peaks emerge, each with very distinct charge densities, as shown in Fig. 6(b). The lowest peak at approximately −8.5 eV resembles a bonding-like orbital that arises from the hybridization between the Si s state and an O p state, with its axis aligned along the Si-O bond. The next peak at approximately −7 eV has a doughnut-shaped charge density arising from a superposition of p-like orbitals. In contrast to an isolated oxygen atom [Figs. 5 and 6(a)],

however, the doughnut-shaped charge density has rotated to become perpendicular to the Si-O bond. This state appears to be a nonbonding orbital as it does not contain any discernible states residing on the Si atom. The highest peak at approximately −6.5 eV resembles the antibonding state of the hybridization between the Si s state and an O p state. This state has charge density on both Si and O, but the charge density is pushed away from the center of the Si-O bond.

For comparison, Fig. 7 shows a schematic hybridization diagram between an s orbital (on the atom on the left) and a p orbital (on the atom on the right). In the diagram in Fig. 7, the intrinsic energy of the s level is lower than that of the p level, similar to the s level of Si and the p levels of O when the two atoms are separated from each other in a Ti crystal. In this scenario, the bonding state is dominated by the s level with excess charge accumulating along the bond. The antibonding state has more of the higher-energy p character with a depletion of charge between the two atoms. The charge densities of Fig. 7 are very similar to those of the states labeled as bonding and antibonding in Fig. 6(b).

Another scenario is also possible in which the intrinsic energy of the p level is lower than that of the s level. In this case the bonding state has more p character, and the antibonding state is more dominated by the s state. This scenario occurs when Al and O are nearest neighbors in a Ti host, as was revealed in Ref. [27] and is shown in Fig. 8.

Figure 8(a) shows the DOS of a supercell of Ti with a substitutional Al and interstitial oxygen beyond their nearest-neighbor shells. In contrast to Si, the Al s levels are above those of the oxygen p levels and are somewhat mixed in with the Ti s levels. When Al is brought into the nearest-neighbor shell of the oxygen, a hybridization between the Al s and O p levels becomes evident [Fig. 8(b)]. A bonding state emerges around −7.7 eV. The charge density associated with this state now has more of a p character since the intrinsic energy of the O p level is below that of the Al s level with which it hybridizes. The next levels around −7.1 eV again have the appearance of nonbonding states, with a doughnut-shaped charge density that is oriented perpendicular to the Al-O bond. The antibonding states are less localized as they also mix with the Ti s levels. Their charge density in the vicinity of the Al-O
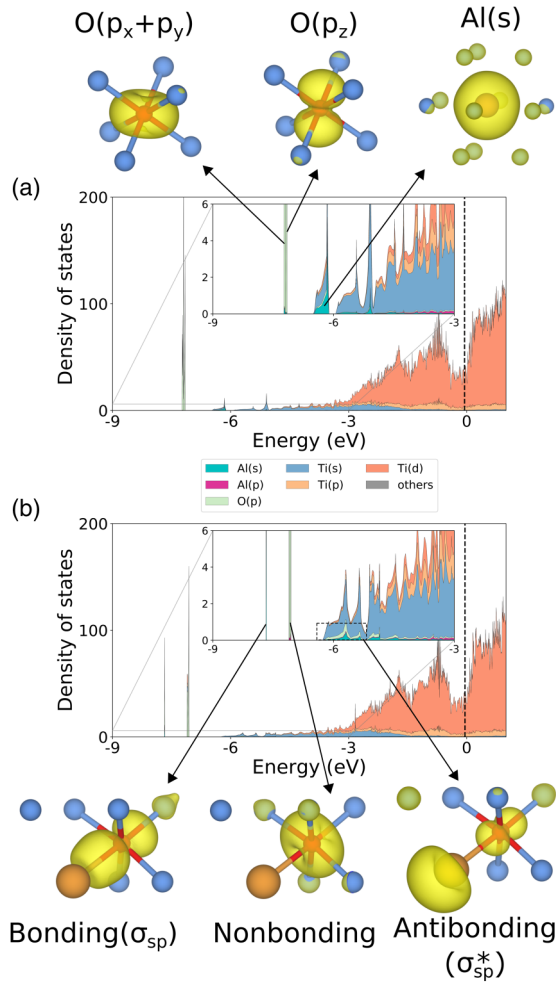
FIG. 8. (a) The DOS of a Ti supercell containing a single substitutional Al in the fourth-nearest-neighbor shell of an interstitial O. (b) The DOS of the same crystal when Al is in the nearest-neighbor shell of an interstitial O.

bond of these states shows features of an s orbital on Al and a p orbital on O, but with a clear depletion of charge at the center of the bond.

For the transition metal alloying elements (i.e., Y, Sc, Zr, Nb, Cr, and Fe), the effects of hybridization are less pronounced. We focus on the Ti-Zr-O system (Fig. 9) as a representative example. The DOS plots of the other transition metal solutes are similar (Fig. 10 and Supplemental Material [49]). When Zr is in the fourth-nearest-neighbor shell of O, the oxygen p levels again resemble those of an isolated oxygen atom in pure Ti, as is evident in Fig. 9(a). In contrast to Si and Al, the Zr valence states are very similar to those of Ti. The Zr valence s and d states are therefore mixed in with those of Ti. The Zr s levels, for example, have energies that are above those of the oxygen p levels, and the difference that separates them is significantly larger than in the case of Si and Al. Hence, the degree of hybridization will be less pronounced when Zr moves into the nearest-neighbor shell of oxygen, as can be seen in Fig. 9(b). The oxygen p levels of an isolated oxygen [Fig. 9(a)] are only slightly modified when Zr becomes a nearest neighbor [Fig. 9(b)]. Two nearly degenerate peaks are evident whose combined charge density has a
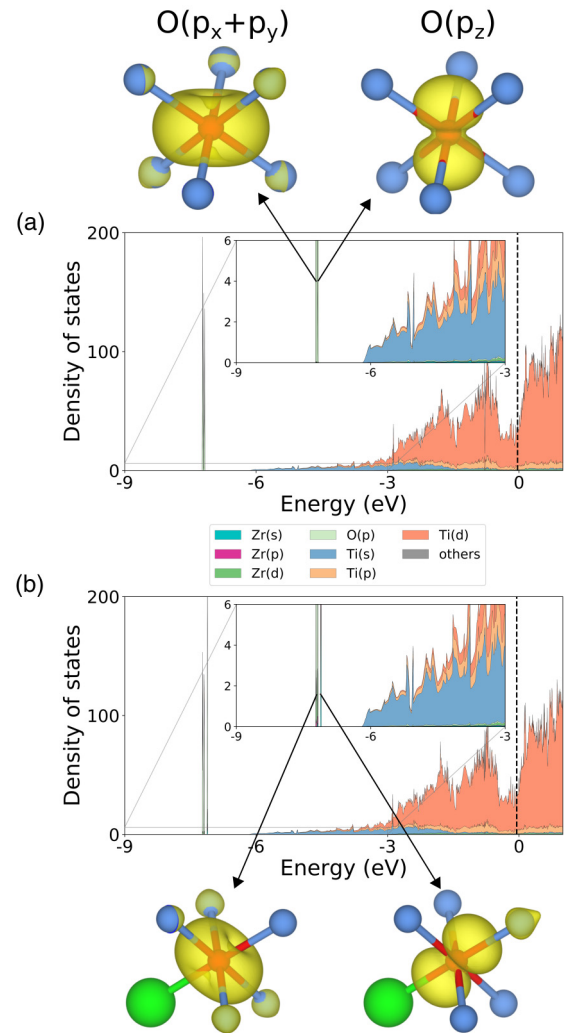

FIG. 9. (a) The DOS of a Ti supercell containing a single substitutional Zr in the fourth-nearest-neighbor shell of an interstitial O. (b) The DOS of the same crystal when Zr is in the nearest-neighbor shell of an interstitial O.

doughnut shape that is almost perpendicular to the X-O bond. A third peak at a slightly higher energy has a charge density of a p-like orbital that is aligned approximately parallel to the X-O bond.

Figure 10 collects the DOS of all the X-O couples when the solute X is within the nearest-neighbor shell of oxygen. The zero on the energy axis of each DOS plot was chosen such that the deep Ti $3s$ level aligns with that of pure Ti. This makes it possible to compare the extent to which different solutes hybridize with the localized O p levels. The effects of transition metal solutes on the oxygen p levels are substantially smaller than those of Al and Si. Figure 10 shows that Nb has the smallest effect on the oxygen levels. For Y, Sc, and Zr, the energy of the peak corresponding to a p-like orbital aligned parallel to the X-O bond is higher than the nearly degenerate pair of peaks with a doughnut-shaped charge density, while for Cr and Fe, these peaks are reversed. Whether the p-like orbital parallel to the X-O bond has a higher or lower energy than the degenerate p states with a doughnut charge density appears to be correlated with the atomic radius of the solute
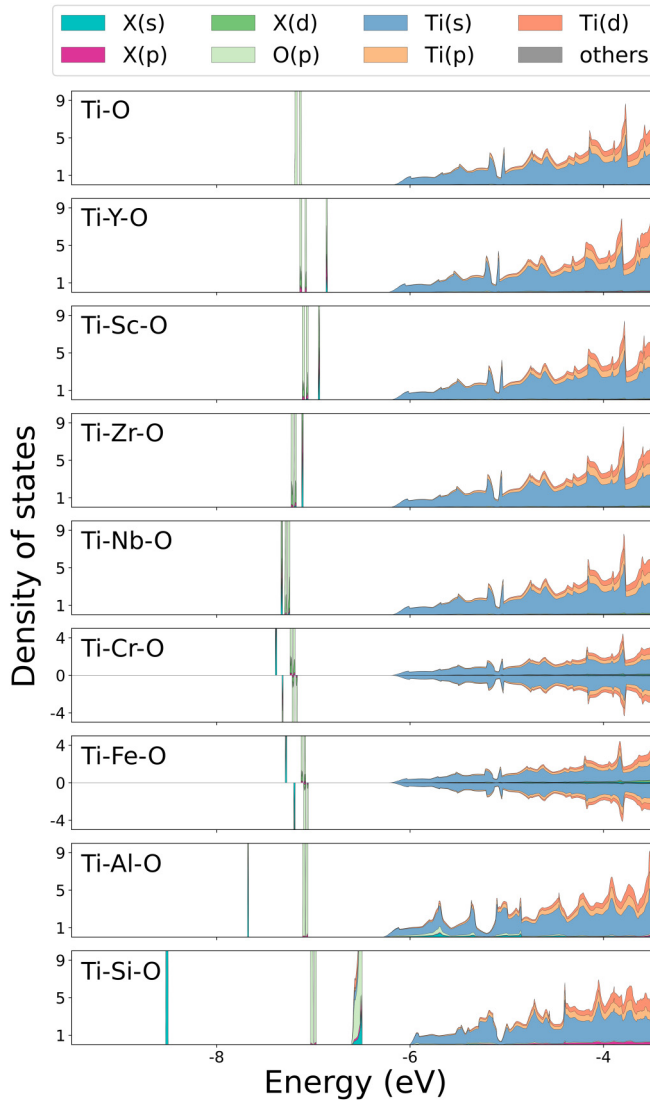
FIG. 10. A compilation of the DOS of a Ti supercell containing a nearest-neighbor X-O pair (X=Y, Zr, Nb, Cr, Fe, Al, and Si). The DOS of a Ti supercell with a single oxygen and no solutes is also shown (top) for comparison. Both the spin-up and spin-down DOSs are shown for Ti supercells containing Cr and Fe as there is a slight degree of spin polarization.

relative to that of Ti (Fig. 1): for the larger solutes (Y, Sc, Zr) the energy is higher, while for the smaller solutes (Nb, Cr, and Fe) the energy is lower.

C. Bader charges of O and X

The energies of the p levels of dissolved oxygen in hcp Ti reside well below the Fermi level and the electronic valence states derived from Ti 4s and 3d levels. Hence, the O p states will draw electrons from the surrounding Ti host, leading to a filled-shell configuration on oxygen and a local accumulation of charge. An accumulation of charge on oxygen is confirmed with calculated Bader charges, which predict a value of -1.4 for an oxygen atom in a $3 \times 3 \times 3$ supercell of hcp Ti. This suggests that the Ti host acts as an electron reservoir from which the dissolved oxygen can draw electrons to achieve a
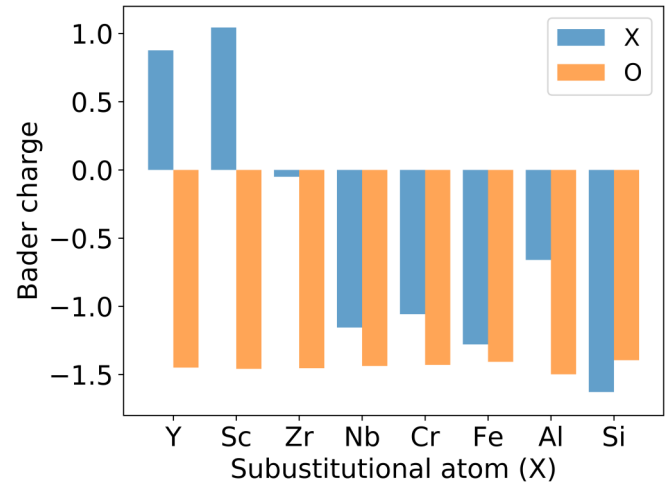

FIG. 11. Calculated Bader charges on different solutes and O in a supercell of hcp Ti when the solute and oxygen are nearest neighbors.

closed-shell configuration. It should be noted that the charge of an atom in a solid is not a well-defined quantity. Bader charges are one way of qualitatively assessing whether an atom accumulates charge or donates it. While the calculated Bader charge of oxygen in Ti is -1.4, which contrasts with a charge of -2 for a closed shell, the calculated DOS plots clearly indicated a closed-shell configuration on the interstitial oxygen with all three valence p states residing well below the Fermi level and therefore fully occupied.

The alloying elements X may also donate or accept charge from the Ti host depending on the intrinsic energies of their valence states relative to those of Ti. Figure 11 collects the calculated Bader charges for the different alloying elements when they are in the nearest-neighbor shell of an interstitial oxygen. The Bader charges of the solutes do not change significantly when they are in the fourth-nearest-neighbor position from oxygen and thereby largely surrounded by Ti. With the exception of Y, Sc, and Zr, all other alloying elements have a negative Bader charge. Y and Sc solutes have a net positive charge, suggesting that they donate charge to the Ti host. Zr solutes have a negligible Bader charge, which is consistent with the fact that Ti and Zr are both group 4 elements and have similar valence electron structures.

The predicted Bader charges suggest the importance of electrostatic interactions between O and X. However, since the Ti host is metallic, any Coulomb interactions between X and O will be strongly screened by the free electrons of the host. It is only when X and O are nearest neighbors, with no intervening Ti, that the net charges on both X and O may lead to strong Coulomb interactions.

IV. DISCUSSION

Alloying elements are often added to Ti to reduce its oxygen solubility. A first-principles study by Wu and Trinkle [26] showed that almost any element from the periodic table that is substitutionally dissolved in hcp Ti will repel interstitial oxygen. Our calculations on a subset of substitutional alloying elements confirm these predictions.

While a simple explanation for a repulsive or attractive interaction between solutes in metals is often difficult to discern from the results of first-principles electronic structure calculations, we can identify several factors that partially explain the trends in the calculated binding energies ΔE of Fig. 3. One interaction is electrostatic in nature and arises from a redistribution of electron density between the Ti host and the solutes that make them charged. Another emerges from local relaxations due to a size mismatch between the substitutional solute and Ti. A third interaction has a quantum mechanical origin that we term a *closed-shell* repulsion and emerges from the hybridization between highly localized and fully occupied oxygen p states and solute valence states. We elaborate further on these interactions.

A remarkable property of Ti is that it does not appear to interact strongly with isolated interstitial oxygen. The energies of the oxygen p levels are far removed from those of the Ti $4s$ and $3d$ levels. The DOS peaks associated with the oxygen p levels (Fig. 5) are very sharp, which is indicative of localized, atomiclike orbitals that hybridize negligibly with the surrounding Ti host. The oxygen p levels are far below the Fermi level and are, therefore, fully filled, leading to a negatively charged, closed-shell configuration around oxygen that is stabilized by the Madelung potential of the surrounding Ti host. The substitutional solutes X are also charged, with Y and Sc donating electrons to the surrounding Ti host, making them positively charged, and other solutes such as Nb, Cr, Fe, Al, and Si drawing electrons from the host, making them negatively charged.

The local accumulation of charge leads to electrostatic interactions between oxygen and the substitutional solutes when they are at close range. While the surrounding metallic Ti host, with its high density of itinerant electrons at the Fermi level, can screen the charges when the solute X and O are at large distances from each other, it will be less effective when they are nearest neighbors. Based on the calculated Bader charges in Fig. 11, we can therefore expect an attractive electrostatic interaction between negatively charged O and positively charged Y and Sc and a repulsive electrostatic interaction between O and the negatively charged solutes Nb, Cr, Fe, Al, and Si. According to Fig. 11, Zr has almost no net charge, which is consistent with the fact that Zr and Ti have very similar valence electron structures. Short-range electrostatic interactions between Zr and O are likely not significant.

Local atomic relaxations are another factor that will contribute to the binding energies in Fig. 3. The effect of relaxations can be inferred from the equilibrium X-O bond distances in Fig. 4. Due to the constraint of the crystal, any increase in the X-O bond length will need to be accommodated by a shortening of the surrounding Ti-O bond distances or a displacement of the solute, both effects leading to a strain energy penalty. Figure 4 shows that the Cr-O bond length is very similar to the opposing Ti-O bond length. Furthermore, the unrelaxed and relaxed binding energies for Cr-O pairs are very similar (Fig. 3), indicating that relaxations are negligible when Cr is in the nearest-neighbor shell of O. All other X-O bond lengths are larger than the equilibrium Ti-O bond length. Hence, with the exception of Cr, local relaxations likely also play an important role in the binding energy between solutes and oxygen in Ti.

The combination of electrostatic interactions and local strain penalties can explain many of the general trends of the binding energies in Fig. 3. While Y and Sc have an attractive electrostatic interaction with oxygen, they have a larger atomic radius than Ti. As is evident in Fig. 4, both Y and Sc strive for a larger X-O distance that compresses the opposing Ti-O bond length and thereby incur a strain energy penalty. In the case of Y, which has a binding energy with O that is close to zero, this strain energy penalty is apparently large enough to fully compensate the attractive electrostatic interaction between Y and O. The binding energy between Sc and O is slightly negative. Sc is smaller than Y, which is reflected in a smaller Sc-O distance when compared to the Y-O distance in Fig. 4. The penalty due to relaxations for the Sc-O pair should therefore be slightly less than that for the Y-O pair. Furthermore, the Sc Bader charge is slightly more positive than that of Y, suggesting a more attractive electrostatic interaction between Sc and O when compared to that between Y and O. The combined effect leads to a small negative binding energy between Sc and O. Since Zr has almost no net charge as it has a valence electronic structure that is very similar to that of Ti, it should have a negligible electrostatic interaction with oxygen. The positive (repulsive) binding energy of a Zr-O bond therefore has its origin in large part in the increased Zr-O distance and compressed Ti-O distances. The positive energy is again consistent with the fact that Zr has a larger atomic radius than Ti. All the remaining solutes (Nb, Cr, Fe, Al, and Si) have a positive binding energy with O, which is consistent with both a repulsive electrostatic interaction and a positive strain energy penalty due to increased X-O bond distances (except Cr).

A remaining puzzle persists, however, with respect to Al and Si. Both Al and Si have smaller atomic radii than Ti. Nevertheless, they favor very large Al-O and Si-O distances and highly compressed Ti-O distances on the opposite side of O. The Si-O distance is especially large and significantly larger than the other X-O distances. The Al-O and Si-O binding energies (Fig. 3) are also significantly larger than those of the other solutes. The larger binding energies cannot be attributed solely to an electrostatic repulsion since the Bader charge of Al is smaller than that of Nb, Cr, and Fe, while that of Si is not much larger in absolute value.

Our analysis of the DOS suggests the existence of a closed-shell repulsive interaction that can explain the peculiarities of Al and Si and its interactions with dissolved oxygen in Ti. As described in Sec. III B, the placement of a substitutional solute, X, in the first-nearest-neighbor shell of an interstitial oxygen atom alters the positions of the oxygen p peaks and the shapes of their associated charge densities. Figure 10 shows that Al and Si induce the largest degree of hybridization. The calculated DOS and charge densities in Figs. 6 and 8 show that the hybridization is primarily between the oxygen p orbitals and the s states of Al or Si. Furthermore, the hybridization between O and Al/Si within Ti leads to clearly discernible bonding and antibonding states. For transition metal solutes, such as Y, Sc, Zr, Nb, Cr, and Fe, the effect is not as pronounced. While similar hybridization phenomena may also occur between oxygen and transition metal solutes, it is less evident from an inspection of the DOS plots in Fig. 10 as the solute states with which O may hybridize are mixed in with those of Ti.

The localized bonding and antibonding states on the Si-O and Al-O pairs are well below the Fermi level of the Ti host and are consequently fully occupied. The deep-lying s and p states should, therefore, behave similarly to those of closed-shell atoms as they approach each other. Since both the bonding and antibonding states are filled, there is no energetic benefit to hybridize and form an attractive bond. Furthermore, closed-shell atoms repel each other at short distances due to increases in the electron kinetic energy and the Pauli exclusion principle as their closed-shell electron clouds begin to overlap.

The existence of a closed-shell repulsion between dissolved oxygen and solutes such as Al and Si can be inferred from the relaxed X-O bond lengths. The bond lengths collected in Fig. 4 show that, while Al and Si are smaller than Ti (Fig. 1), the relaxed Al-O and Si-O distances are significantly larger than a nearest-neighbor Ti-O bond. We interpret this as arising from a strong repulsion between the closed-shell O p and Al/Si s orbitals. The Ti-O bond lengths opposite those of the Al-O or Si-O bonds are very short (Fig. 4), especially when compared to the Ti-O bond distances when O is next to a transition metal solute such as Nb, Cr, or Fe. The degree with which these Ti-O bonds are compressed is a measure of the strength of the closed-shell O-X repulsion since the X-O bond length will continue to relax (i.e., lengthen) until it is countered by an equal force by the opposing Ti-O bond. Based on these arguments, we concluded that the closed-shell repulsion is especially strong for Al-O and Si-O bonds and offers an explanation as to why the Al-O and Si-O binding energies are much larger than those of Nb, Cr, and Fe, which have similar Bader charges.

The concept of a closed-shell repulsion, as is understood for atoms and molecules, is unlikely a general phenomenon for solutes within a metal due to the high density of itinerant electrons. It is, however, a useful description of the interaction between O and Al or Si solutes in hcp Ti as these particular solutes have highly localized atomiclike orbitals that do not hybridize with the metallic host but do form very clear bonding and antibonding states below the Fermi level that are fully filled. Nevertheless, the parallel with atoms and molecules only goes so far, as the Bader charge on O is not strictly -2, but rather closer to -1.4, indicating that a portion of the electrons in the bonding and antibonding states is delocalized.

While a closed-shell repulsion may also contribute to the binding energies between the other solutes and oxygen, it is not as evident from the DOS in Fig. 10. If it is present, its effects will be less significant. Nevertheless, the degree of hybridization between O and X (as evident in the changes in the O p levels) may explain differences among the Nb-O, Cr-O, and Fe-O binding energies. While both Nb and Fe have similar Bader charges (Fig. 11) and similar Nb-O and Fe-O distances (Fig. 4), the Fe-O binding energy is almost twice as large as that between Nb and O. The binding energy between Cr and O is also larger than that of Nb-O, even though the Cr-O bond length has a negligible strain energy penalty and Cr has a smaller Bader charge than Nb. As is clear in Fig. 10, Nb has the smallest effect on the O p levels, suggesting a negligible degree of hybridization. Fe and Cr, in contrast, do cause peak splitting that is qualitatively similar to that of Al, but to a much lesser degree. This hybridization may also produce a closed-shell repulsive interaction between O and

Fe/Cr that is similar to, but smaller than, that between O and Al, leading to larger repulsive binding energies for the Cr-O and Fe-O pairs compared to that of the Nb-O pair. Other, more subtle interactions undoubtedly also play a role, but they are more difficult to identify.

As a final note, we point out that the alloying elements considered in this study interact very differently with Ti at nondilute concentrations. To some degree, the behavior at nondilute concentrations can be correlated with the atomic size differences and the calculated Bader charges. The Ti-Y phase diagram consists of large two-phase regions with very little Y solubility in hcp and bcc Ti [50]. The reason is likely the large size mismatch between Ti and Y. Zr and Ti are completely miscible, while Nb can dissolve into hcp Ti up to several atom percent below the Ti hcp-bcc transition temperature before forming a large bcc solid solution. In contrast to the early transition metals, Cr, Fe, Al, and Si are strong compound formers with Ti. Cr combines with Ti to form the stable Cr_2Ti Laves phase [44], while Fe has minimal solubility in hcp Ti and forms the stable TiFe intermetallic with the B2 structure [51]. The solubility of Si in hcp Ti is small and quickly leads to the formation of Ti_3Si, a line compound, whereas the solubility of Al in hcp is much larger and leads to the formation of Ti_3Al, which exists over a range of compositions [52,53]. It is likely no coincidence that this trend correlates with a steady increase in the X-O binding energy and an appreciable negative Bader charge on the solutes X upon going to the right in the periodic table. Nb is again an exception, with a negative Bader charge in the dilute limit, but nevertheless forming a solid solution with Ti.

V. CONCLUSION

We have used first-principles electronic structure methods to shed light on the nature of the interactions between oxygen and dilute solutes in hcp Ti. By focusing on representative elements from different parts of the periodic table, we have identified distinct interaction types that in combination produce a short-range repulsion between most substitutional solutes and interstitial oxygen in hcp Ti. One interaction type is electrostatic in nature and arises from a transfer of electron density to the solutes from the Ti host. A strain penalty is also present due to a size mismatch between the solute and the Ti host. Another interaction identified in this work, which is especially pronounced for Al and Si solutes, is similar to the repulsion between closed-shell atoms at short distances and becomes more pronounced with an increase in the degree of hybridization between atomiclike orbitals on oxygen and the solute. We expect that the interactions among solutes identified in this study may also play an important role in many other alloys, especially multiprinciple element alloys made of refractory metals that tend to dissolve high concentrations of interstitial species such as O, N, and C.

[1] J. Abriata, J. Garces, and R. Versaci, Bull. Alloy Phase Diagrams **7**, 116 (1986).

[2] J. L. Murray and H. A. Wriedt, J. Phase Equilib. **8**, 148 (1987).

[3] H. Okamoto, J. Phase Equilib. Diffus. **32**, 473 (2011).

[4] H. J. Goldschmid, *Interstitial Alloys* (Butterworth, London, 1967).

[5] A. Salamat, A. L. Hector, P. Kroll, and P. F. McMillan, Coord. Chem. Rev. **257**, 2063 (2013).

[6] B. Paul Burton, A. van de Walle, and H. T. Stokes, J. Phys. Soc. Jpn. **81**, 014004 (2011).

[7] B. P. Burton and A. van de Walle, CALPHAD: Comput. Coupling Phase Diagrams Thermochem. **39**, 97 (2012).

[8] B. P. Burton and A. van de Walle, CALPHAD: Comput. Coupling Phase Diagrams Thermochem. **37**, 151 (2012).

[9] B. Puchala and A. Van der Ven, Phys. Rev. B **88**, 094108 (2013).

[10] M.-H. Chen, B. Puchala, and A. Van der Ven, CALPHAD: Comput. Coupling Phase Diagrams Thermochem. **51**, 292 (2015).

[11] N. S. H. Gunda and A. Van der Ven, Phys. Rev. Mater. **2**, 083602 (2018).

[12] N. S. H. Gunda, B. Puchala, and A. Van der Ven, Phys. Rev. Mater. **2**, 033604 (2018).

[13] C. R. Weinberger and G. B. Thompson, J. Am. Ceram. Soc. **101**, 4401 (2018).

[14] Q. Yu, L. Qi, T. Tsuru, R. Traylor, D. Rugg, J. Morris, M. Asta, D. Chrzan, and A. M. Minor, Science **347**, 635 (2015).

[15] M. Ghazisaeidi and D. Trinkle, Acta Mater. **76**, 82 (2014).

[16] Y. Chong, M. Poschmann, R. Zhang, S. Zhao, M. S. Hooshmand, E. Rothchild, D. L. Olmsted, J. Morris, D. C. Chrzan, M. Asta, and A. M. Minor, Sci. Adv. **6**, eabc4060 (2020).

[17] P. Kofstad, P. Anderson, and O. Krudtaa, J. Less-Common Met. **3**, 89 (1961).

[18] P. Kofstad, J. Less-Common Met. **12**, 449 (1967).

[19] G. Bertrand, K. Jarraya, and J. Chaix, Oxid. Met. **21**, 1 (1984).

[20] J. Unnam, R. Shenoy, and R. Clark, Oxid. Met. **26**, 231 (1986).

[21] A. M. Chaze and C. Coddet, J. Mater. Sci. **22**, 1206 (1987).

[22] K. L. Luthra, Oxid. Met. **36**, 475 (1991).

[23] A. Rahmel and P. J. Spencer, Oxid. Met. **35**, 53 (1991).

[24] G. P. Kelkar and A. H. Carim, J. Am. Ceram. Soc. **78**, 572 (1995).

[25] H. Seifert, A. Kussmaul, and F. Aldinger, J. Alloys Compd. **317-318**, 19 (2001).

[26] H. H. Wu and D. R. Trinkle, J. Appl. Phys. **113**, 223504 (2013).

[27] N. S. H. Gunda and A. Van der Ven, Acta Mater. **191**, 149 (2020).

[28] G. Kresse and J. Hafner, Phys. Rev. B **47**, 558 (1993).

[29] G. Kresse and J. Hafner, Phys. Rev. B **49**, 14251 (1994).

[30] G. Kresse and J. Furthmüller, Comput. Mater. Sci. **6**, 15 (1996).

[31] G. Kresse and J. Furthmüller, Phys. Rev. B **54**, 11169 (1996).

[32] J. P. Perdew, K. Burke, and M. Ernzerhof, Phys. Rev. Lett. **77**, 3865 (1996).

[33] P. E. Blöchl, Phys. Rev. B **50**, 17953 (1994).

[34] G. Kresse and D. Joubert, Phys. Rev. B **59**, 1758 (1999).

[35] E. Sanville, S. D. Kenny, R. Smith, and G. Henkelman, J. Comput. Chem. **28**, 899 (2007).

[36] W. Tang, E. Sanville, and G. Henkelman, J. Phys.: Condens. Matter **21**, 084204 (2009).

[37] G. Henkelman, A. Arnaldsson, and H. Jónsson, Comput. Mater. Sci. **36**, 354 (2006).

[38] K. Momma and F. Izumi, J. Appl. Crystallogr. **44**, 1272 (2011).

[39] J. C. Slater, J. Chem. Phys. **41**, 3199 (1964).

[40] O. Senkov, J. M. Scott, S. V. Senkova, D. B. Miracle, and C. F. Woodward, J. Alloys Compd. **509**, 6043 (2011).

[41] T. M. Butler, K. J. Chaput, J. R. Dietrich, and O. N. Senkov, J. Alloys Compd. **729**, 1004 (2017).

[42] D. B. Miracle and O. N. Senkov, Acta Mater. **122**, 448 (2017).

[43] O. N. Senkov, D. B. Miracle, K. J. Chaput, and J.-P. Couzinie, J. Mater. Res. **33**, 3092 (2018).

[44] A. R. Natarajan, P. Dolin, and A. Van der Ven, Acta Mater. **200**, 171 (2020).

[45] R. J. Pérez and A. R. Massih, J. Nucl. Mater. **360**, 242 (2007).

[46] F. H. Stott, G. C. Wood, and J. Stringer, Oxid. Met. **44**, 113 (1995).

[47] K. Chou, P.-W. Chu, C. G. Levi, and E. A. Marquis, J. Mater. Sci. **52**, 9884 (2017).

[48] K. Chou, P.-W. Chu, and E. A. Marquis, Corros. Sci. **140**, 297 (2018).

[49] See Supplemental Material at http://link.aps.org/supplemental/10.1103/PhysRevMaterials.5.073604 for density of states and the charge densities of orbitals in hcp Ti supercell with interstitial oxygen and substitutional transition metal solutes (Y, Sc, Nb, Cr, Fe).

[50] K. Gupta, J. Phase Equilib. Diffus. **30**, 402 (2009).

[51] J. L. Murray, Bull. Alloy Phase Diagrams **2**, 320 (1981).

[52] J. C. Schuster and M. Palm, J. Phase Equilib. Diffus. **27**, 255 (2006).

[53] M. Fiore, F. Beneduce Neto, and C. R. d. F. Azevedo, Mater. Res. **19**, 942 (2016).